Electronic Structure of $Rh_2(\mu\text{-}CO)(CO)_2(H_2PCH_2PH_2)_2$. An Example of a Non-A-Frame Structure

Carles Bo,[†] Miquel Costas,[†] Josep M. Poblet,*[,†] Marie-Mad. Rohmer,[‡,§] and Marc Benard*[,‡]

Departament de Química, Universitat Rovira i Virgili, Pç Imperial Tàrraco 1, 43005 Tarragona, Spain, Laboratoire de Chimie Quantique, UPR 139 du CNRS, Université Louis Pasteur, F-67000 Strasbourg, France, and Applications Scientifiques du Calcul Intensif (ASCI), UPR 9029 du CNRS, Orsay, France

Received April 28, 1995[⊗]

Calculations based on density functional theory (DFT) and Hartree−Fock configuration interaction (HF-CI) methodology have been carried out to investigate the rhodium−rhodium coupling in $Rh_2(CO)_2(dppm)_2$, **1** (dppm = $Ph_2PCH_2PPh_2$) and in $Rh_2(\mu\text{-}CO)(CO)_2(dppm)_2$, **2**. DFT geometries, obtained with the Dgauss program, are in good agreement with those determined from X-ray, but HF geometries, calculated using the same basis sets, yield bond distances systematically too long. Calculations indicate that the rhodium atoms in **1** are linked by a single bond. The insertion of a semibridging carbonyl between the two metal atoms leads to a shortening of the rhodium−rhodium distance and also to a noticeable weakening of the metal−metal interaction. Both effects, and also the stabilization of the HOMO of **2**, are related to an observed change from square planar to tetrahedral of the ligand environment of the Rh atom proximal to the inserted CO. Both MO analysis and bond characterization from the topology of the charge density confirm the existence of a bonding interaction between the semibridging carbonyl and the distal rhodium atom. The electronic structures of the dicationic complex $[Rh_2(CO)_3(dppm)_2]^{2+}$ and of the A-frame-like, isoelectronic system $Rh_2Br_2(\mu\text{-}CO)(dppm)_2$ are also discussed. The electron deformation density is derived from **2** by means of several methodological approaches, namely, HF, HF-CI, DFT, and DFT + gradient corrections. The HF deformation density obtained in the plane containing the metals and the three CO ligands is discussed, as well as the "correlation density" obtained from the difference maps DFT − HF and CI − HF.

Introduction

Bimetallic complexes with A-frame structure were first reported in 1977.[1−3] A frames are M_2L_2L' complexes, the metals being held close to each other by bidentate dppm or dpam bridging ligands (dppm = $Ph_2PCH_2PPh_2$, dpam = $Ph_2AsCH_2AsPh_2$) and L′ being a ligand at the apex of the "A", see structure I. L′, which occupies a symmetric position between

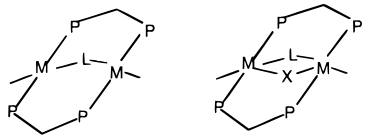

I II

the two metal centers, can be an atom or a small molecule[4] but also a larger system such as N−((*p*-NO_2)Ph).[5] Many complexes of this class can add a molecule to yield the structure shown schematically as II.

The addition of CO to $Rh_2(CO)_2(dppm)_2$, **1**, forms $Rh_2(\mu\text{-}CO)(CO)_2(dppm)_2$, **2**.[6] Although Eisenberg's group in their first report proposed an A-frame structure (I) for **2**,[6] some years later the X-ray characterization[7] showed that the structure of **2** is highly distorted with respect to the symmetric C_{2v} A frame. The two rhodium atoms present different coordination environments, the bridging carbonyl being responsible for the distortion. In fact, this ligand may be described as weakly semibridging (sb). More recently, the same distortion has been observed in $RhM(\mu\text{-}CO)(CO)_2(dppm)_2$, M = Co [8] and Ir,[9] isoelectronic with **2**. Homobimetallic cobalt[10] and iridium[11] analogues of **2** have also been synthesized. The bridging carbonyl streching frequency in $Co_2(CO)_3(dppm)_2$ suggests a more symmetric structure for the cobalt compound.[10] The main feature of $Ni_2(CO)_3(dppm)_2$, a dimer with two electrons more, is the unusual cis configuration of the dppm ligands.[12]

Variable temperature NMR experiments[7] suggest that the A-frame structure in fluxional complexes is an intermediate in Scheme 1.

Protonation of **2** yields $[Rh_2(\mu\text{-}H)(\mu\text{-}CO)(CO)_2(dppm)_2]^+$,[13] which has the same number of electrons as **2**, but in this case the carbonyl exhibits a symmetrically bridging nature, evidencing again the fluxionality of the apex carbonyl.

Hoffman and Hoffmann[14] have shown that the assignment of a metal−metal bond order in A frames requires an accurate

† Universitat Rovira i Virgili.
‡ Université Louis Pasteur.
§ UPR 9029 du CNRS.
⊗ Abstract published in *Advance ACS Abstracts,* May 1, 1996.

(1) Kubiak, C. P.; Eisenberg, R. *J. Am. Chem. Soc.* **1977**, *99*, 6129.
(2) Olmstead, M. M.; Hope, H.; Benner, L. S.; Balch, A. L. *J. Am. Chem. Soc.* **1977**, *99*, 5502.
(3) Brown, M. P.; Puddephatt, R. J.; Rushid, M.; Seddon, K. R. *Inorg. Chim. Acta* **1977**, *23*, L27.
(4) Puddephatt, R. J.; Azam, K. A.; Hill, R. H.; Brown, M. P.; Nelson, C. D.; Moulding, R. P.; Seddon, K. R.; Grossel, M. C. *J. Am. Chem. Soc.* **1983**, *105*, 5642, and references cited therein.
(5) Ge, Y.-W.; Peng, F.; Sharp, P. R. *J. Am. Chem. Soc.* **1990**, *112*, 2632.
(6) Kubiak, C. P.; Eisenberg, R. *J. Am. Chem. Soc.* **1980**, *102*, 3637.
(7) Woodcock, C.; Eisenberg, R. *Inorg. Chem.* **1985**, *24*, 1285.
(8) Elliot, D.; Fergusson, G.; Holah, D. G.; Hughes, A. N.; Jennings, M. C.; Magnuson, V. R.; Potter, D.; Puddephatt, R. J. *Organometallics* **1990**, *9*, 1336.
(9) Mc Donald, R.; Cowie, M. *Inorg. Chem.* **1990**, *29*, 1564.
(10) Lisic, E. C.; Hanson, B. E. *Organometallics* **1987**, *6*, 512.
(11) Sutherland, B. R.; Cowie, M. *Organometallics* **1985**, *4*, 1637.
(12) Osborn, J. A.; Stanley, G. G.; Bird, P. H. *J. Am. Chem. Soc.* **1988**, *110*, 2117.
(13) Kubiak, C. P.: Woodcock, C. Eisenberg, R. *Inorg. Chem.* **1982**, *21*, 2119.

S0020-1669(95)00525-8 CCC: $12.00

Scheme 1

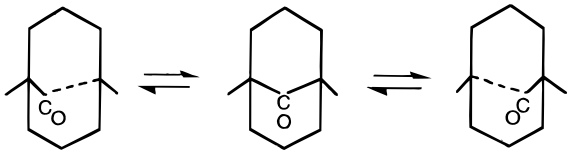

analysis of the molecular orbitals. Frequently, the formal bond order does not coincide with that deduced from MO analysis. Several electronic configurations can be assigned to the asymmetric structure: (16e−18e) assuming a single Rh−Rh bond, (18e−18e) with a double bond, and (16e−16e) without a metal−metal bond. Such a variability in the formal electronic structure makes even more complicated the analysis from elemental electron counting.

Several authors have described the metal−carbonyl interaction in organometallic complexes.[15−18] All agree with Cotton's original hypothesis that bridging and semibridging carbonyls accept density from the metal d orbitals into their π^* orbital. The goal of the present paper is to discuss the nature of the metal−metal and metal−semibriging carbonyl interactions in a non-A-frame complex like **2** and in its precursor **1**. Various methodological approaches should be used in order to enlighten various aspects of the same bonding situation. One electron methods like extended Hückel (EH) provide a qualitative picture of the fragment orbital interactions responsible for the stability of the molecule in its equilibrium position. However, neither a geometry optimization nor a distribution of the electron density can be relied on at this level of theory. Quantitative information concerning those properties as well as energy barriers should be sought from ab initio methodology, which includes the density functional theory (DFT) and the Hartree−Fock methodology (HF, or HF-CI if correlation is accounted for through configuration interaction). Within this more eleborate framework, we have shown that the theory of atoms in molecules, developed by Bader and co-workers,[19,20] can be useful in the metal−metal[21a] and in the metal−carbonyl[21b] bond characterization. The electronic structure will be discussed by means of molecular orbital analysis and topological analysis of charge density. A comparison between DFT and HF methods in the study of binuclear complexes is also reported.

Theoretical Details

SCF calculations based on DFT and HF methodologies were carried out for complexes $Rh_2(CO)_2(H_2PCH_2PH_2)_2$, **3**, and $Rh_2(\mu\text{-}CO)(CO)_2(H_2PCH_2PH_2)_2$, **4**, taken as models for **1** and **2**, respectively. DFT calculations were performed with the DGauss[22] program, whereas HF calculations were done with the ASTERIX[23] and TURBOMOLE[24] systems of programs. The basis sets used are the DZVP[25] sets taken from the DGauss library, which are Gaussian type basis sets of split valence plus polarization quality. The sizes of those basis sets are (9s,5p,1d) for C and O and (12s,8p,1d) for P, contracted into [3,2,1] and [4,3,1], respectively. The basis set for Rh is a (18s,12p,9d) set contracted into [6,5,3], and for H atoms (5s) contracted into [2]. DFT calculations were done self-consistently by using the local density approximation for the exchange-correlation potential in the form given by Vosko, Wilk, and Nusair (VWN),[26] also called the LSD potential. Perturbative nonlocal functional corrections (NLSD) were applied to the LSD-SCF geometries. The nonlocal functional used in this work includes the gradient corrected exchange term proposed by Becke[27] and the correlation term proposed by Perdew[28] (Becke−Perdew, or BP model). The topological properties of ρ were investigated with a version of the AIMPAC package.[29]

$Rh_2(\mu\text{-}CO)(CO)_2(H_2PCH_2PH_2)_2$ Geometry Optimization

Full geometry optimizations were done at the LSD and HF levels for complex **4**. Selected parameters are given in Table 1, and a perspective view is provided in Figure 1. The geometries optimized at LSD[30] and BP[31] levels are in good agreement with the experimental structures for mononuclear transition metal complexes as well as for binuclear systems with metal−metal interactions, as shown by Ziegler in a series of pioneering papers. The computed Rh−Rh distance of 2.746 Å is longer, by no more than 0.007 Å, than the experimental parameter reported for **2**. The Rh−P bond lengths are also accurately determined by the DFT method. We can see from Table 1 that the rhodium−terminal carbonyl bond distances are rather well reproduced, the discrepancies being below 0.03 Å. The Rh−C bond distance for the semibridging carbonyl was computed to be 1.912 Å, whereas the corresponding X-ray value for **2** is 1.857 Å. The largest deviation concerning the bond distances is related to the weak interaction between the semibridging carbonyl and the distal metal center: the Rh−Rh′−C_{sb} angle is 4.7° smaller than the experimental one, leading to a Rh−C_{sb} distance of 2.231 Å. This value confirms the nonsymmetric nature of the carbonyl, but it is shorter by 0.3 Å than the distance observed from X-rays. HF distances are worse than DFT ones in all cases. On the contrary, the angles obtained at the HF level are better than those corresponding to DFT calculations: the angular discrepancies are below 4° at the HF level but can reach 10° at the DFT level. Both calculations confirm the pyramidal conformation of the ligands surrounding the proximal metal center, Rh′. The P′−Rh′−P′ angle is computed to be 113.6° (DFT) or 107.3° (HF). The observed value for this angle is 104.4°. The position of the terminal CO is in keeping with this pyramidalization (Table 1). In contrast with the structure of a trigonal pyramid observed around Rh′,

(14) Hoffman, D. M.; Hoffmann, *R. Inorg. Chem.* **1981**, *20*, 3543.
(15) Cotton, F. A. *Prog. Inorg. Chem.* **1976**, *21*, 1.
(16) Jemmis, E. D.; Pinhas, A. R.; Hoffman, R. *J. Am. Chem. Soc.* **1980**, *102*, 2576.
(17) (a) Bénard, M.; Dedieu, A.; Nakamura, S. *Nouv. J. Chim.* **1984**, *8*, 149. (b) Casarin, M.; Ajo, D.; Granozzi, G.; Tondello, E.; Aime, S. *Inorg. Chem.* **1985**, *24*, 1241.
(18) (a) Morris-Sherwood, B. J.; Powell, C. B.; Hall, M. B. *J. Am. Chem. Soc.* **1984**, *106*, 5079. (b) Sargent, A. L.; Hall, M. B. *J. Am. Chem. Soc.***1989**, *111*, 1563. (c) Sargent, A. L.; Hall, M. B. *Polyhedron* **1990**, *9*, 1799. (d) Simpson, C. Q., II; Hall, M. B. *J. Am. Chem. Soc.* **1992**, *114*, 1641.
(19) Bader, R. F. W. *Chem. Rev.* **1991**, *91*, 893.
(20) Bader, R. F. W. *Atoms in Molecules. A Quantum Theory*; Clarendon Press: Oxford, U.K., 1990.
(21) (a) Bo, C.; Poblet, J.-M.; Bénard, M. *Chem. Phys. Lett.* **1990**, *169*, 89. (b) Bo, C.; Sarasa, J. P.; Poblet, J. M. *J. Phys. Chem.* **1993**, *97*, 6362.
(22) *UNICHEM*, Version 2.1-Dgauss; Publication APG 5505−2.1; Cray Research Inc, Mendota Heights, 1993.
(23) (a) Ernenwein, R.; Rohmer, M.-M.; Bénard, M. *Comput. Phys. Commun.* **1990**, *58*, 305. (b) Rohmer, M.-M.; Demuynck, J.; Bénard, M.; Wiest, R.; Bachmann, C.; Henriet, C.; Ernenwein, R. *Comput. Phys. Commun.* **1990**, *60*, 127. (c) Wiest, R.; Demuynck, J.; Bénard, M.; Rohmer, M.-M.; Ernenwein, R. *Comput. Phys. Commun.* **1991**, *62*, 107.
(24) Ahlrichs, R.; Bär, M.; Häser, M.; Horn, H.; Kölmel, C. *Chem. Phys. Lett.* **1989**, *162*, 165.
(25) Godbout, N.; Salahub, D. R.; Andzelm, J.; Wimmer, E. *Can. J. Chem.* **1992**, *70*, 560.
(26) Vosko, S. H.; Wilk, L.; Nusair, M. *Can. J. Phys.* **1980**, *58*, 1200.
(27) (a) Becke, A. D. *Phys. Rev. A* 1988, *38*, 3098. (b) Becke, A. D. *J. Chem. Phys.* **1988**, *88*, 2547.
(28) Perdew, J. P. *Phys. Rev. B* **1986**, *33*, 8822.
(29) Biegler-Konig, F. W.; Bader, R. F. W.; Tang, T. H. *J. Comput. Chem.* **1982**, *3*, 317.
(30) (a) Sosa, C.; Andzelm, J.; Elkin, B. C.; Wimmer, E.; Dobbs, K. D.; Dixon, D. A. *J. Phys. Chem.* **1992**, *96*, 6630. (b) Fan, L.; Ziegler, T. *J. Phys. Chem.* **1992**, *96*, 6937, and references cited therein.
(31) (a) Fan, L.; Ziegler, T. *J. Am. Chem. Soc.* **1992**, *114*, 10890. (b) Folga, E.; Ziegler, T. *J. Am. Chem. Soc.* **1993**, *115*, 5169.

Table 1. Selected Bond Distances (Å) and Bond Angles (deg) for $Rh_2(\mu\text{-}CO)(CO)_2(H_2PCH_2PH_2)_2$ (DG, density functional; HF, Hartree−Fock)

Distances

	calc^{DG}	calc^{HF}	expt	calc^{DG}(C_{2v})		calc^{DG}	calc^{HF}	expt	calc^{DG}(C_{2v})
Rh−Rh′	2.746	2.921	2.739	2.720	Rh′−C′	1.897	2.037	1.881	1.878[b]
Rh′−C_{sb}	1.912	1.919	1.857	2.079[b]	Rh−C	1.871	2.007	1.842	
Rh−C_{sb}	2.231	2.758	2.533		C_{sb}−O_{sb}	1.182	1.138		1.176
Rh′−P′	2.327	2.464	2.320[a]	2.305[b]	C′−O′	1.167	1.123		1.171[b]
Rh−P	2.293	2.421	2.300[a]		C−O	1.167	1.118		

Angles

	calc^{DG}	calc^{HF}	expt	calc^{DG}(C_{2v})		calc^{DG}	calc^{HF}	expt	calc^{DG}(C_{2v})
P−Rh−P	165.1	167.6	166.7	150.6[b]	Rh−C−Rh′	70.7	74.9	75.5	
P′−Rh′−P′	113.6	107.3	104.4		Rh−Rh′−C_{sb}	58.8	65.7	63.5	
C′−Rh′−P′	100.6	102.3	101.1	91.4[b]	C_{sb}−Rh′−C′	99.2	99.2	99.6	
C−Rh−Rh′	171.8	177.9	177.1	167.8[b]	O_{sb}−C_{sb}−Rh	119.2	114.4	116.8	139.1[b]
C′−Rh′−Rh	152.8	164.9	161.4		O_{sb}−C_{sb}−Rh′	158.2	170.7	167.8	

[a] Averaged values. [b] Note that some geometric parameters are equivalent by symmetry.

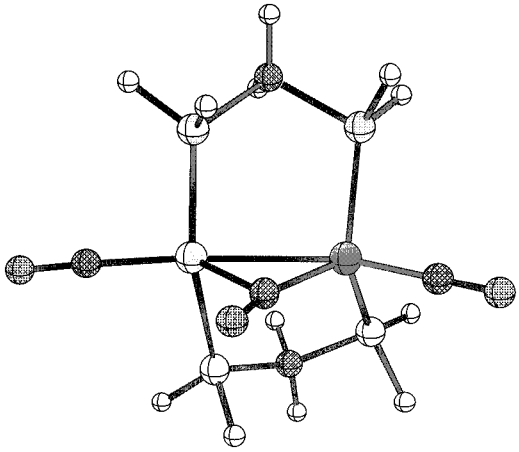

Figure 1. Representation of $Rh_2(\mu\text{-}CO)(CO)_2(H_2PCH_2PH_2)_2$, **4**.

the conformation of the diphosphine and of the terminal carbonyl remains close to planarity near the distal rhodium atom, Rh (Table 1).

In order to compute the energy barrier associated with the fluxional displacement of the semibridging carbonyl represented in Scheme 1, a C_{2v} structure can be considered as the intermediate with highest energy. The C_{2v} geometry was fully optimized at the LSD level, leading to the bond distances and bond angles collected in Table 1. The Rh−Rh distance was found to be slightly shorter than that in the C_s geometry, and the other parameters seem to be in agreement with chemical intuition. The value of 2.079 Å computed for the rhodium−bridging carbonyl bond distance clearly indicates the symmetrization of the metal−carbonyl interactions with respect to the C_s conformation, in which the corresponding bond distances are 1.912 and 2.231 Å. Rhodium−bridging carbonyl distances in related complexes range between 1.96 Å in $Rh_2Br_2(\mu\text{-}CO)(dppm)_2$[32] to 2.15 Å in $[Rh_2(\mu\text{-}H)(\mu\text{-}CO)(CO)_2(dppm)_2]^+$.[13] Note that the P−Rh−P and C−Rh−Rh′ angles optimized for this symmetric conformation are representative of a trend toward a pyramidal arrangement of the ligands.

The energy difference between the optimal structures with C_s and C_{2v} symmetries is 10.1 kcal/mol at the LSD level and 11.2 kcal/mol at the BP level. Those computed barriers compare well with the value of $\Delta G^{\ddagger}$ experimentally determined from variable temperature NMR experiments,[7] since the free energy associated with the coalescence of proton signals was estimated to be 12 kcal/mol.

(32) Cowie, M.; Dwight, S. K. *Inorg. Chem.* **1980**, *19*, 2508.

Table 2. Bond Properties Computed for $Rh_2(\mu\text{-}CO)(CO)_2(H_2PCH_2PH_2)_2$ (All Values in atomic units)

bond	ρ_b	$\nabla^2\rho_b$	ϵ	d_{A-B}[a]
Rh−C_{sb}	0.078	0.166	0.061	2.261−1.957
Rh′−C_{sb}	0.148	0.413	0.096	1.986−1.627
Rh−C	0.157	0.527	0.036	1.930−1.606
Rh′−C′	0.147	0.527	0.001	1.946−1.638
Rh−P	0.096	0.175	0.063	2.150−2.183
Rh−P′	0.090	0.171	0.014	2.218−2.179
C−O	0.431	0.415	0.011	0.754−1.451
C′−O′	0.431	0.396	0.002	0.754−1.470
C_{sb}−O_{sb}	0.418	0.275	0.001	0.764−1.470

[a] Distance from the bond critical point to atom A and to atom B.

Topological Properties of ρ

Table 2 summarizes the bond properties computed for **4**. In the terminology classically used to interpret the topology of the charge density,[19,20] the properties of a bond are characterized by the parameters ρb (charge density at the bond critical point, bcp), $\nabla 2\rho$b (Laplacian of the charge density at the bcp that coincides with the sum of the three curvatures of the Hessian matrix), and ϵ (ellipticity of the density). The characterization of bond critical points linking the semibridging carbonyl with both rhodium atoms stresses the bridging nature of this ligand. With reliance still on Bader's criteria, the absence of a bcp between the two metal centers implies the lack of a direct metal−metal interaction. We will then discuss the influence of the semibridging carbonyl on the Rh−Rh interaction in this kind of complex. The values obtained for $\nabla 2\rho$ at the bcps for Rh−P and Rh−C bonds are positive and relatively large, evidencing a certain closed shell interaction. Similar results were described in theoretical studies of other organometallic and coordination complexes using HF wave functions.[21,33]

The main difference between the structures with C_s and C_{2v} symmetries concerns the metal−metal interaction, characterized as a bond critical point in the C_{2v} geometry. No such bcp is found in the complex with C_s symmetry. It could be argued that the reduction of the Rh−Rh distance from 2.746 (C_s) to 2.720 Å (C_{2v}) increases the overlap between the rhodium atoms and by this way the additional charge density induces the formation of a bond critical point. Low and co-workers,[34] in a study on the metal−metal bond in $Co_2(CO)_8$, have discussed the appearence of a bond critical point as a function of the Co−Co distance. They found that no bcp was present at the

(33) (a) Lin, Z.; Hall, M. B. *J. Am. Chem. Soc.* **1992**, *114*, 2928. (b) Costas, M.; Bo, C.; Poblet, J. M. *Chem. Phys. Lett.* **1992**, *200*, 8.

(34) Low, A. A.; Kunze, K. L.; MacDougall, P. J.; Hall, M. B. *Inorg. Chem.* **1991**, *30*, 1079.

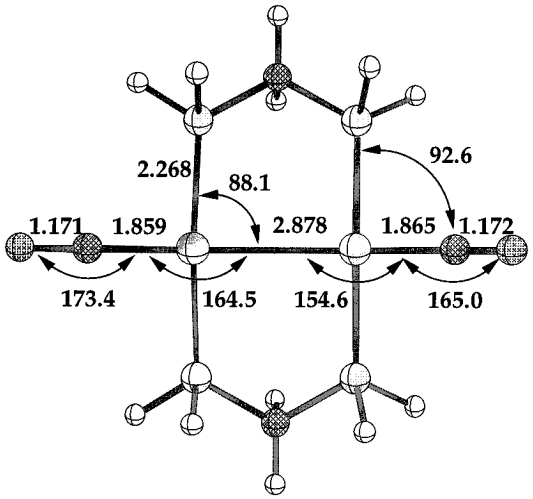

Figure 2. Representation of $Rh_2(CO)_2(H_2PCH_2PH_2)_2$, **3**.

experimental geometry, but a slight shortening of the Co−Co distance was sufficient for the bcp to show up.

LSD calculations have also been carried out on **3**, the parent complex of **4**. The Rh−Rh separation in **3** is 2.878 Å. To our knowledge, no X-ray determination has appeared in the literature for this compound. Electron counting rules require the presence of a single metal−metal bond in order to achieve a 16 electron count in the valence shell of each metal atom. In this case, a bond critical point was located within the intermetal region ($\rho_b = 0.042$ e/au^3, $\nabla 2\rho_b = 0.025$ e/au^5), in perfect agreement with traditional electron counting. The bcp was characterized even though the Rh−Rh bond length is larger by 0.13 Å than the metal−metal distance obtained for **4**, for which no bcp could be obtained. Perspective view of **3**, including selected parameters, is displayed in Figure 2. Addition of one CO molecule to complex **3** leads to complex **4**. At the LSD level the energy released by process $Rh_2(CO)_2(H_2PCH_2PH_2)_2 + CO \rightarrow Rh_2(CO)_2(H_2PCH_2PH_2)_2$ has been calculated to be 57.1 kcal/mol. No direct experimental information exists in order to check this reaction energy. Nevertheless, DFT M−C bond energies[31,35] seem, in general, consistent with experimental bond enthalpies.[36] As stated by Hoffmann[14] "conventional electron counting would predict no bond (perhaps double bond) for **4**". In that work, Hoffman and Hoffmann studied symmetric A-frame complexes and analyzed MO interaction diagrams, discussing conflicts between electron counting schemes and the MO picture of bonding in this type of complex.

What is the reliability of those conclusions obtained from Bader's analysis? The point is controversial since it has been noticed that this method is sensitive to small changes in the basis set, geometry, and account of the electron correlation. Part of the criticism addressed to Bader's analysis often comes from the ill-conditioned character of the analyzed density distribution. It is well-known that ab initio calculations carried out using minimal or unbalanced basis sets and without accounting for the most important correlation effects will yield poor results whatever may be the method used to analyze the wave function. As far as the geometry is concerned, Bader specifies that the analyzed density distribution *must* be associated with the optimal geometry of the considered system.[20] Note that this condition is fulfilled in the present work. Furthermore, the density obtained from DFT calculations includes correlation effects and the used basis sets are of reasonable quality. In spite of those necessary precautions, it is not excluded that the topological analysis of the density displays a basic instability, the best example of such a behavior being the case of $Co_2(CO)_8$ investigated by Low and colleagues.[34] In this case, the instability is to be traced to the very nature of the metal−metal interaction—a weak bent bond—and not to the method used for its analysis.

Chart 1

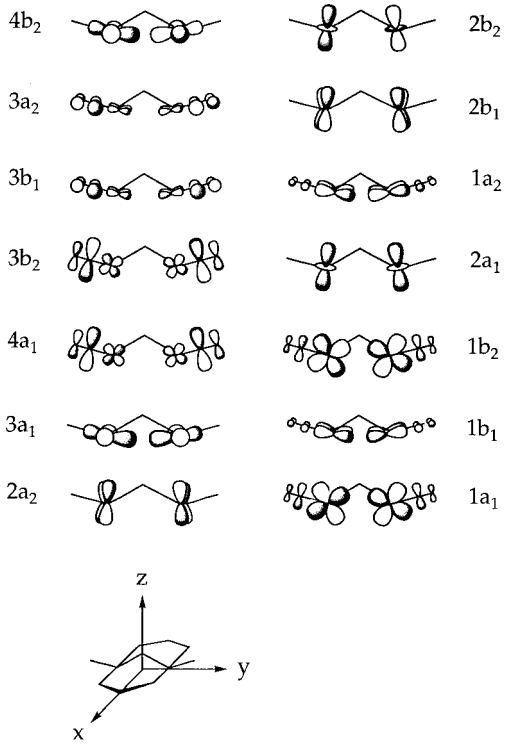

MO Fragment Analysis

In order to describe the metal−metal bonding features of $Rh_2(\mu\text{-}CO)(CO)_2(H_2PCH_2PH_2)_2$, extended Hückel calculations have been carried out. The interaction diagram between the orbitals of a symmetric M_2L_6 fragment, which are sketched in Chart 1, and the apex CO orbitals is shown in Figure 3, assuming for the complex the C_{2v} symmetry. The orbitals which are not directly involved in the M−M bonding have not been displayed for clarity. The 3a1 orbital is the key MO to be borne in mind when analyzing the bonding in $Rh_2(\mu\text{-}CO)(CO)_2(H_2PCH_2PH_2)_2$.

Chart 1 shows that the eight underlying fragment orbitals appear as metal−metal bonding−antibonding pairs: $1a_1/1b_2$, $1b_1/1a_2$, $2a_1/2b_2$, and $2b_1/2a_2$. Next in energy, fragment orbital $3a_1$ displays a metal−metal σ-bonding character when a symmetric conformation is assumed for the complex. This orbital is destabilized by a repulsive interaction with the lone pair of the semibridging CO. The orbitals with b_2 symmetry, including $3b_2$, are stabilized through back-donation towards the appropriate π^* orbital of the sb CO. This destabilization of $3a_1$ (HOMO) combined with a stabilization of $3b_2$ (LUMO) results in a relatively small HOMO−LUMO gap in the symmetric form of $Rh_2(\mu\text{-}CO)(CO)_2(H_2PCH_2PH_2)_2$. Meanwhile the HOMO is still looking basically like the filled dimetal fragment orbital, and the LUMO stems from the bonding combination between the $3b_2$ component and the apex π^* b_2 orbital and, to a lesser extent, from the antibonding counterpart of the $2b_2$-π^*CO. The d-metal character of the LUMO is close to 50%. Moreover in the C_{2v} geometry, the M_2L_6 fragment

(35) Ziegler, T. *Chem. Rev.* **1991**, *91*, 651.
(36) Martinho Simões, J. A.; Beauchamp, J. L. *Chem. Rev.* **1990**, *90*, 629.
(37) (a) Bader, R. F. W.; Gillespie, R. J.; MacDougall, P. J. *J. Am. Chem. Soc.* **1988**, *110*, 7329. (b) Gillespie, R. J.; Bytheway, I.; DeWitte, R. S.; Bader, R. F. W. *Inorg. Chem.* **1994**, *33*, 2115.

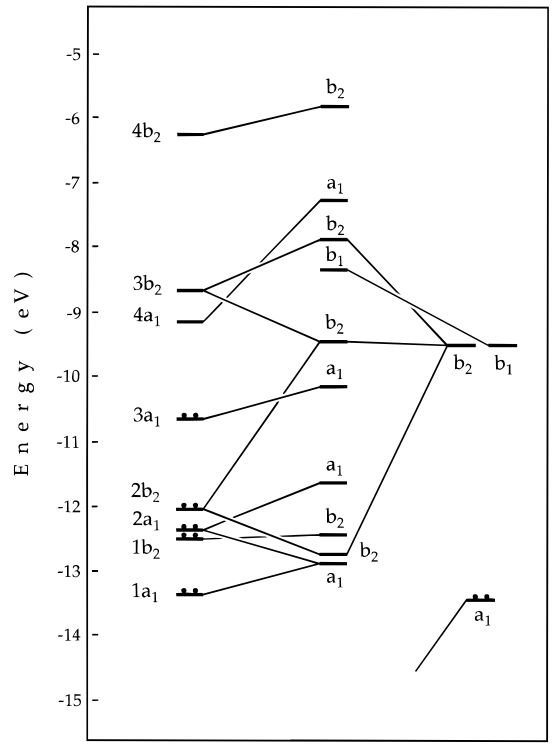

Figure 3. Molecular orbital interaction diagram for **4**, assuming a symmetrically bridging carbonyl and C_{2v} symmetry, from extended Hückel calculations. Left-hand side: fragment orbitals of **3**, as displayed in Chart 1 (orbitals antisymmetric with respect to the plane of the carbonyls have not been represented for clarity). Right-hand side: frontier orbitals of the symmetrically bridging carbonyl.

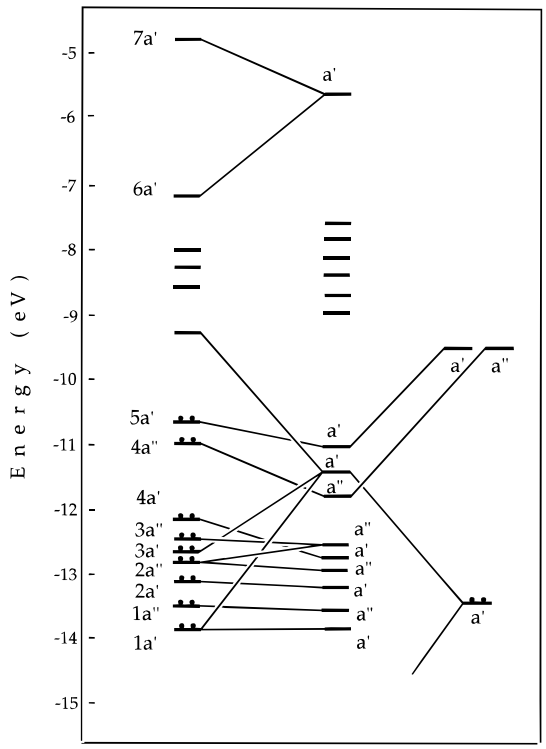

Figure 4. Molecular orbital interaction diagram for **4**, with the observed structure represented in Figure 1 (C_s symmetry, semibridging carbonyl, and pyramidal environment of the proximal rhodium atom) from extended Hückel calculations. Left-hand side: orbitals of the dimetal fragment, as displayed in Chart 2. Right-hand side: frontier orbitals of the semibridging carbonyl.

orbitals with b_1 symmetry are not properly oriented for giving rise to an important mixing with the empty π^*_{CO} orbital of the same symmetry.

The last filled orbital ($3a_1$) emerges as the main one responsible for the net Rh−Rh bond and therefore for the presence of a bcp in the charge distribution linking the two Rh centers, when the C_{2v} symmetry is assumed for the complex. However, the presence or the lack of a metal−metal bond between electron-rich metal centers may be difficult to detect from the set of *occupied* metal orbitals, where the interaction can be scattered among various MOs of same symmetry. In the present case of a d^9−d^9 interaction, only one orbital formally attributed to the dimetal entity will remain unoccupied. This orbital, $4b_2$, is clearly metal−metal antibonding in the dimetal fragment with C_{2v} symmetry (Chart 1). This analysis of the unoccupied orbital $4b_2$, unaffected by the approach of the symmetrically bridging CO, is sufficient to prove the existence of a net metal−metal bonding character in the *occupied* set of metal orbitals with a1 symmetry. This Rh−Rh bond is not sufficient however to ensure the stability of the symmetric conformation due to the four electron, destabilizing interaction which develops between the bridging CO lone pair and the Rh−Rh bonding orbital $3a_1$.

We now consider the relaxation of the system from C_{2v} to C_s. The tilting of the central carbonyl from a bridging to a semibridging position is accompanied by a pyramidalization of the ligand environment of the metal atom Rh′ facing the CO lone pair. The changes induced by this pyramidalization in the orbital set of the dimetal fragment are displayed in Chart 2. The interaction diagram of those fragment orbitals with COsb are displayed in Figure 4. Fragment orbitals labeled as a_1 and b_2 in the C_{2v} fragment are presently gathered in the a′ representation. Fragment orbital 5a′, which is the equivalent of $3a_1$, is now mainly centered on the proximal rhodium atom,

Chart 2

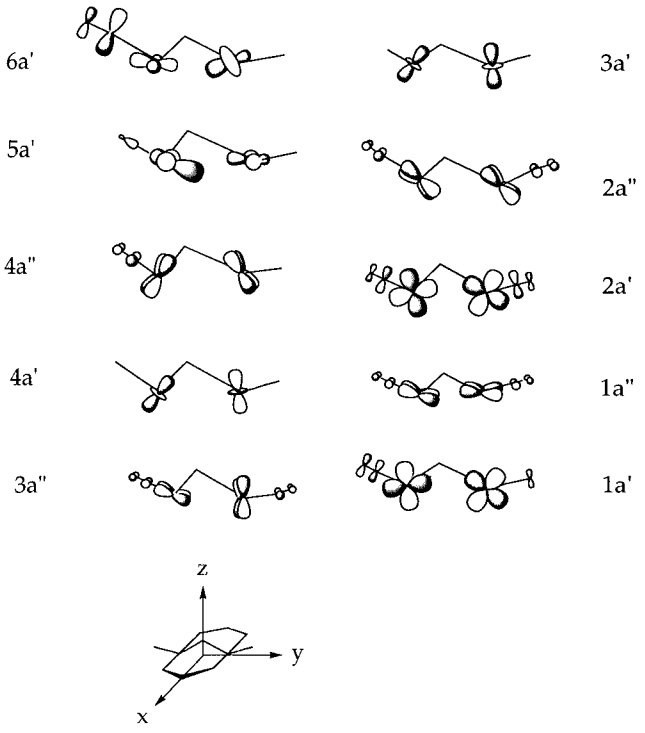

with a minor contribution from the other metal. This fragment orbital can still be considered as metal−metal bonding, but the different contributions of both metals and the tilt of the lobe centered on Rh′, induced by the orientation of the terminal carbonyl, largely decrease the bonding overlap (Chart 2). The highest, unoccupied metal fragment orbital 6a′ appears as the counterpart of 5a′ with a loosely antibonding Rh−Rh character

Chart 3

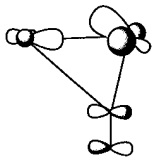

and a most important contribution from the distal rhodium atom Rh. This MO analysis is in complete agreement with the conclusions derived from the topology of the DFT charge density. The structural asymmetry of complex **4** now allows for a stabilization of the HOMO 5a′, represented in Chart 3, through a mixing with the π^* orbital of CO previously referred to as b_2. The distortion also reduces the repulsion between the metal−metal bond electrons and the CO lone pairs. This repulsion has been transferred to the d_{z^2}-like orbital of the pyramidal fragment and results in the occupied orbital next to the HOMO, also belonging to the a′ representation (Figure 4).

MO analysis reveals electronic reasons that favor the distorted geometry. If we now remember the results of the topological analysis, we can observe how they agree with the logics of extended Hückel interacting orbitals. The lack of a bcp linking the rhodium atoms in the C_s geometry may be explained by the partial loss of direct metal−metal coupling due to the CO distortion and to the ligand pyramidalization around Rh′. As Low and co-workers have pointed out for $Co_2(CO)_8$, a certain metal−metal interaction can be compatible with the absence of a bcp in the intermetal region.[34] In fact, Figure 4 indicates that a certain interaction persists between the two metal centers in the occupied set of MOs with a′ symmetry. Notice that there does not exist a direct relationship between the metal−metal distance and the presence of a net metal−metal coupling. Hence, whereas **3** (Rh−Rh = 2.878 Å, C_{2v}) and **4** (Rh−Rh = 2.72 Å, C_{2v} symmetry assumed) exhibit metal−metal bonds, **4** (Rh−Rh = 2.746 Å, C_s) does not show such interaction.

Laplacian of Charge Density

It has been shown by many authors that the Laplacian function of charge density can be used to investigate electronic structure and bonding.[20,21,33,38] In a previous work,[21] we have found that the Laplacian of charge density provides a criterion aimed at ascertaining the bridging nature of a carbonyl ligand. The valence shell of the oxygen atom in a bridging carbonyl displays two maxima of charge concentration like a ketonic oxygen, whereas a single lone pair is found for the oxygen atom of a terminal carbonyl. These conclusions were taken from the analysis of $Fe_2(CO)_9$. In the same work, the charge density distribution of $Fe_2(CO)_6(C_2H_2)$ was also studied, and one of the carbonyl ligands was described as semibridging. In that case, the valence shell of the oxygen atom also displays two lone pairs, separated by an angle whose value defines the tendency to bridge. However, in $Fe_2(CO)_6(C_2H_2)$ no bcp could be detected between the carbonyl carbon and the distal metal center. This was attributed to the geometry designed for the model molecule.

Complex **4** presents a semibridging carbonyl, and it is linked to both metal atoms by two bond paths, but the valence shell of the oxygen atom now exhibits an unique charge concentration. As stated by several authors[38] in $Fe_2(CO)_9$, the π back-donation to $\pi^*_\perp$ (perpendicular to the metal−metal−carbon plane) is much smaller than to the $\pi^*_{||}$ (parallel to the M−M−C plane), and because of the different population of the π atomic orbitals two charge concentrations appear in the $\pi^*_{||}$ plane. The main difference in **4** is that metal orbitals are available in both planes and initiate similar back-donation interactions toward $\pi^*\perp$ and $\pi^*_{||}$. Hence, the charge density distribution around the semibridging carbonyl remains cylindrical as in a terminal carbonyl.

Electronic Structure of $[Rh_2(CO)_3(H_2PCH_2PH_2)]^{2+}$

Very recently, the dicationic complex $[Rh_2(CO)_3(dppm)_2]^{2+}$ has been obtained via chemical oxidation of $Rh_2(\mu\text{-}CO)(CO)_2(dppm)_2$.[39] The geometric and electronic analysis of this cationic complex can be useful to check our interpretation of the nature of the rhodium−rhodium coupling in complex **4**. If the two ionized electrons in **4** are just leaving the HOMO without major reorganization of the molecular orbitals, two direct consequences must be expected: (i) the bridging carbonyl should occupy a symmetric distribution between the two rhodium atoms since the main origin of the distortion, that is, the repulsion between the carbon lone pair and the metal−metal bonding electrons of fragment orbital $3a_1$, has disappeared; (ii) the Rh−Rh bond length in the dicationic complex should be longer than in its neutral C_{2v} parent since the metal−metal bonding orbital of the neutral system is now unoccupied. DFT calculations carried out for $[Rh_2(\mu\text{-}CO)(CO)_2(H_2PCH_2PH_2)_2]^{2+}$, **5**, fully confirm these assumptions. The geometry of the charged system has been calculated to belong to the C_{2v} symmetry point group, one carbonyl ligand occupying a bridging position between the two rhodium centers. The computed Rh−Rh bond length is 2.829 Å, longer by 0.11 Å than in its neutral parent (2.720 Å). The Rh−CO(bridging) bond distance has been calculated to be 1.998 Å. The nonexistence of a bond critical point linking the two rhodium centers confirms the vanishing of the metal−metal interaction with respect to the C_{2v} conformation of the neutral complex. One is reminded that such a critical point was detected for the symmetric conformation of **4**. Another interesting feature of the $[Rh_2(\mu\text{-}CO)(CO)_2(H_2PCH_2PH_2)_2]^{2+}$ geometry is that upon oxidation the value of the P−Rh−P angle has increased up to 175° (instead of 165° in the neutral complex), the dppm P atoms occupying a trans disposition as in A-frame systems. However, the terminal carbonyls form a relatively small angle with the bridging carbonyl (C−Rh−C = 123°). This makes the structure distinct from dppm-bridged A−frame complexes. A minimum corresponding to the A-frame geometry has been looked for, but the optimization process has always led back to the structure depicted in Figure 5. The geometry obtained for **7** is in contrast with that reported for the isoelectronic compound $Rh_2Br_2(\mu\text{-}CO)(H_2PCH_2PH_2)_2)_2$, **6**. The structure of this latter complex is A-frame-like with an optimized metal−metal bond length of 2.720 Å, a value which is very close to that determined from X-ray for $Rh_2Br_2(\mu\text{-}CO)(dppm)_2$ (2.756 Å).[32] The topological analysis of the charge density reveals the presence of a bcp in the intermetal region, thus confirming $Rh_2Br_2(\mu\text{-}CO)(dppm)_2$ as a d^8-d^8 species having a single Rh−Rh bond.

In order to discuss the electronic properties of **5** and **6**, the fragment orbitals of the A-frame-like fragment $Rh_2Br_2(H_2PCH_2PH_2)_2$ are displayed in Chart 4. The lack of π^* orbitals in the bromine terminal ligands removes the back-bonding interactions. The change in the orientation of the terminal ligands, which allows for a more efficient stabilization of the bridging carbonyl, should be traced to the vanishing of those interactions. A comparison between the $M_2L_2L'_4$ fragment orbitals displayed in Chart 1 for the non-A-frame structure (L = CO) and in Chart

(38) (a) Summerville, R. H.; Hoffman, R. *J. Am. Chem. Soc.* **1979**, *101*, 3821. (b) Bauschlicher, Jr., C. W. *J. Chem. Phys.* **1986**, *84*, 872. (c) Mealli, C.; Proserpio, D. M. *J. Organomet. Chem.* **1990**, *386*, 203.

(39) Shafiq; Eisenberg. *J. Org. Chem.* **1994**, *472*, 337.

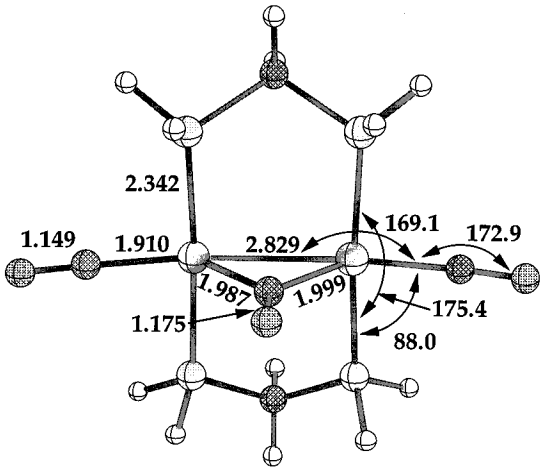

Figure 5. Representation of $[Rh_2(\mu\text{-CO})(CO)_2(PH_2CH_2PH_2)_2]^{2+}$, **7**.

Chart 4

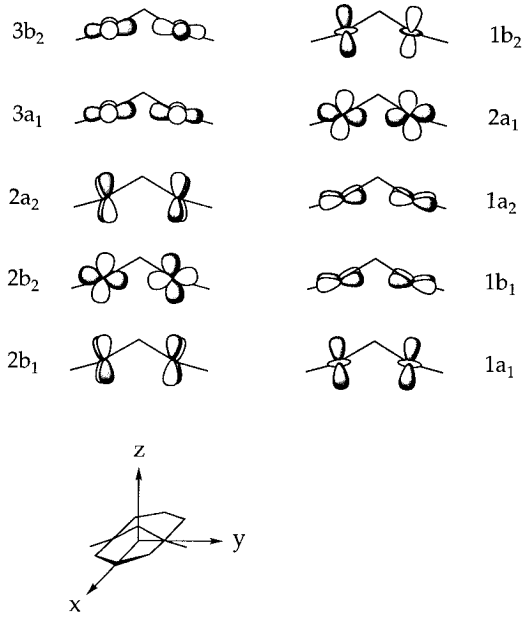

4 for the A-frame-like geometry (L = Br) shows that the orbitals stabilized in Chart 1 by back-donation interactions have their energy raised in Chart 4. More specifically, orbital $1a_1$, the deepest metal orbital in Chart 1, is raised to fourth position in Chart 4 and becomes $2a_1$. In a similar way, antibonding orbital $1b_2$ of Chart 1 is interchanged with orbital $2b_2$. Those orbitals $2a_1$ and $2b_2$ are further destabilized in the A-frame structure because of repulsive interactions with the σ lone pairs of the bromine ligands.

We come now to the interactions between the fragment orbitals of Charts 1 and 4 with the orbitals of the bridging CO ligand and their consequences relative to the metal−metal bonding in complexes **5** and **6**. The interaction diagram concerning the dication **5** can be taken from Figure 3, except that fragment orbital $3a_1$ and its destabilized equivalent in the CO-bridged complex are now unoccupied. In the neutral complex with C_{2v} structure, this HOMO with a1 symmetry was at the origin of the metal−metal bond, on the one hand, and of the small HOMO-LUMO gap, on the other hand. Removing an electron pair from this complex suppresses the metal−metal bond but provides the cation with more thermodynamic stability (Figure 3). In molecule **6**, the modified orientation of the ligands and the new ordering of the metal fragment orbitals result in more efficiency for stabilizing the occupied frontier orbitals of the symmetrically bridged complex (Figure 6).

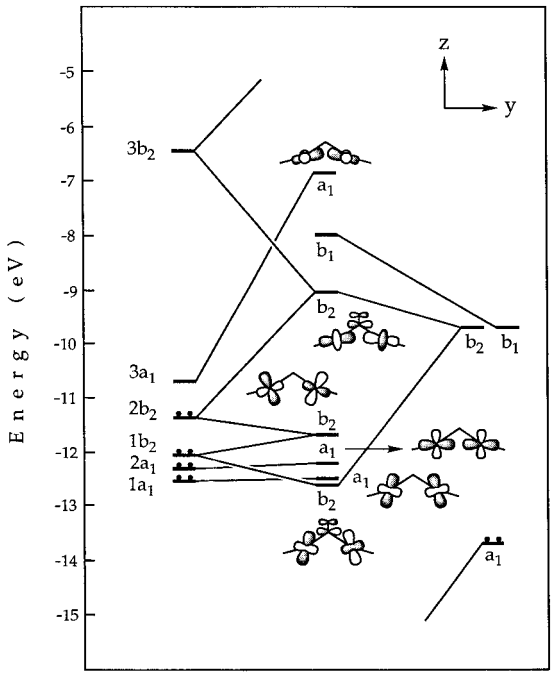

Figure 6. Molecular orbital interaction diagram for $Rh_2Br(\mu\text{-CO})(CO)_2(H_2PCH_2PH_2)_2$ (from extended Hückel calculations).

Fragment orbitals $1a_1$ and $2a_1$ of Chart 4 are no more than slightly destabilized since they are not oriented anymore toward the apex site. Molecular orbital $1a_1$ is an in-phase, but almost nonbonding, combination of metal d_{z^2} orbitals. Molecular orbital $2a_1$ is a bonding combination of metal σ orbitals. Both remain practically unmodified with respect to the corresponding fragment orbitals. The antibonding character of the interaction with the CO lone pair is almost totally transferred to orbital 3a1, now unoccupied and strongly destabilized. MO $1b_2$ represents the bonding combination between the out-of-phase combination of the d_{z^2} orbitals of rhodium and the properly oriented CO π^* orbital. A subtle modification of the balance between metal−metal bonding and antibonding occupied orbitals occurs through molecular orbital $2b_2$ (Figure 6). This orbital remains mainly centered on the metal atoms but incorporates some d_{z^2} shape from fragment orbital $1b_2$ and then becomes stabilized by losing most of its metal−metal antibonding character. The σ-antibonding feature is transferred to molecular orbital $3b_2$. The destabilization of this latter orbital is partly offset by a favorable interaction with the CO π^* orbital, thus allowing this $3b_2$ MO to become the LUMO of complex **6** (Figure 6). To summarize, we are left with a bonding/antibonding pair of metal orbitals ($1b_1/1a_2$, unmodified with respect to Chart 4), three frontier MOs practically nonbonding, as far as the Rh−Rh coupling is concerned ($1b_2$, $1a_1$, $2b_2$; Figure 6), and one σ-bonding combination ($2a_1$). This latter orbital is responsible for the metal−metal bond in **6** predicted by topological analysis.

Electron Density Distributions

Electron Density Differences with Respect to a Promolecule of Spherical Atoms. Figure 7 represents the electron density difference map obtained for complex **2** by subtracting from the total density computed at the Hartree−Fock level the density of a promolecule composed of a superposition of neutral, noninteracting atoms in their ground state.[40] The plane represented in Figure 7 contains the two rhodium atoms and the two terminal and the semibridging carbonyls. The deformation

(40) *Electron Distributions and the Chemical Bond*; Coppens, P., Hall, M. B., Eds.; Plenum Press: New York, 1981.

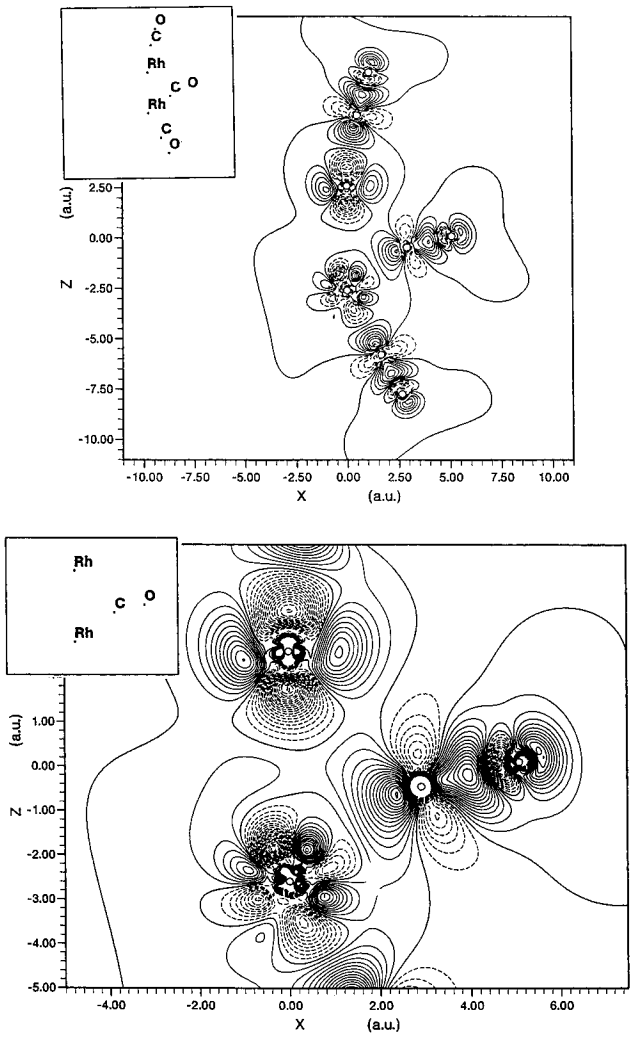

Figure 7. Electron deformation density map computed for **4** with respect to a promolecule composed of noninteracting, neutral, spherically averaged atoms in their ground state. The represented plane contains the two rhodium atoms and the three carbonyls. Solid lines: zero and positive contours (relative charge accumulation). Dashed lines: negative contours (relative charge depletion). (a) Contour interval: 0.1 e/Å^{-3}. (b, bottom) zoom with contour interval 0.05 e/Å^{-3}.

pattern is typical of donation and back-donation interactions as previously discussed for terminal,[40,41] bridging, and semibridging[17a,34] carbonyl complexes. σ donation of terminal carbonyls is evidenced by a relative excess of density in front of the carbon atom (the lone pair) facing a depleted region near the metal (the acceptor orbital). Note that the σ-donation pattern appears less clearly between the semibridging and the proximal rhodium atom, since the carbon lone pair is facing a relatively populated area in the environment of the proximal rhodium atom. At variance from the density distribution around the other metal, the depleted region around the proximal rhodium is quadrifid in the plane of the three carbonyls. Although one of the four depleted lobes is approximately oriented toward the lone pair of the semibridging CO, this narrow and shallow region of electron depopulation cannot compare with the large density holes facing the lone pairs of the terminal carbonyls (Figure 7). This should be related to the orbital interaction diagram of Figure 4, evidencing the repulsive interaction between the lone pair of the semibridging carbonyl and the occupied d_{z^2}-like orbital of the proximal rhodium atom in a trigonal pyramid environment. Note that in spite of the semibridging conformation of the central CO, Figure 7b suggests that part of the σ donation remains oriented toward the *distal* rhodium atom. The π^* acceptor orbital of the CO ligands shows up as a pair of depleted lobes centered on the carbon atoms. Metal donating orbitals appear as density peaks facing them in the π position. Each metal atom is in position to simultaneously back-donate to one terminal and to the semibridging carbonyl.

The question of the metal−metal bond is difficult to discuss from the sole criterion of the deformation density with respect to a promolecule of spherical atoms.[34,40] Density accumulations associated with the overlap of 3d orbitals are often at the limit of significancy, and the peak >0.05 e/Å^{-3} obtained in the region where a bent Rh−Rh bond could be expected (Figure 7b) would have been used as an argument in favor of such a coupling would it be corroborated from orbital or topological analysis. We have seen that this is not the case. However, a closer look at Chart 3 shows that this representation of the HOMO in the semibridged complex does not exclude a weak overlap precisely in the region where the wide, "peninsular" accumulation is obtained (Figure 7b).

"Correlation density": DFT − HF and CI − HF Density Maps. Hartree−Fock and Kohn−Sham molecular orbitals are both eigenvectors of a one-electron Hamiltonian, but the different definitions of those operators lead to distinct interpretations for the MOs.[42] It is therefore of interest to compare the density distributions and the related properties obtained for both types of wave functions. Such a comparison has already been carried out by Wang and colleagues.[43] In this latter work, the density distribution of the carbon monoxide molecule and its Laplacian computed from HF and from post-HF calculations carried out at several levels of accuracy were compared to the DFT calculations corrected by the Becke−Perdew or Perdew−Wang−Perdew functionals. A similar investigation has been recently carried out by Laidig on a series of small molecules (HCl, H_2O, HCN).[44] In spite of the success of DFT calculations in modeling the properties of metal complexes and clusters, no such comparison has been reported yet between HF, correlated HF, and DFT-like calculations for metal-containing molecules, except for the work of Hrusak and colleagues[45] more specifically focused on the geometries and energetics of cationic gold complexes, and for the very recent study of Wang and colleagues on the nitrido−chromium(V) complex [Cr^V (bpb)N] with bpb = 1,2-bis(2-pyridinecarboxamido)benzene.[46] The comparison between Hartree−Fock SCF and DFT density distributions computed in this latter work reveals important differences at the quantitative, and even at the qualitative, level, but most of the discrepancies should be attributed to the different quality of the Gaussian basis sets used in both calculations. More specifically, the lack of polarization functions in the basis set used for the HF calculation explains the poor quality of the density distribution obtained at that level of calculation expecially in the plane of the chromium−nitrogen triple bond.[46] Our goal in the present study is then a comparison of the electron density computed for complex **2** at the HF, HF + CI, DFT (or

(41) (a) Kok, R. A.; Hall, M. B. *J. Am. Chem. Soc.* **1985**, *107*, 2599. (b) Sherwood, D. E.; Hall, M. B. *Inorg. Chem.* **1983**, *22*, 93. (c) Spasojevic-de Biré, A.; Nguyen, Q. D.; Strich, A.; Thieffry, C.; Bénard, M. *Inorg. Chem.* **1990**, *29*, 4908. (d) Baert, F.; Guelzim, A.; Poblet, J.-M.; Wiest, R.; Demuynck, J.; Bénard, M. *Inorg. Chem.* **1986,** *25*, 1830.

(42) Parr, R. G.; Yang, W. *Density Functional Theory of Atoms and Molecules*; Oxford University Press: New York, 1989.

(43) Wang, J.; Shi, Z.; Boyd, R. J.; Gonzalez, C. A. *J. Phys. Chem.* **1994**, *98*, 6988.

(44) Laidig, K. E. *Chem. Phys. Lett.* **1994**, *98*, 285.

(45) Hrusàk, J.; Hertwig, R. H.; Schröder, D.; Schwerdtfeger, P.; Koch, W.; Schwarz, H. *Organometallics* **1995**, *14*, 1284.

(46) Wang, C.-C.; Wang, Y.; Chou, L.-K.; Che, C.-M. *J. Phys. Chem.* **1995**, *99*, 13899.

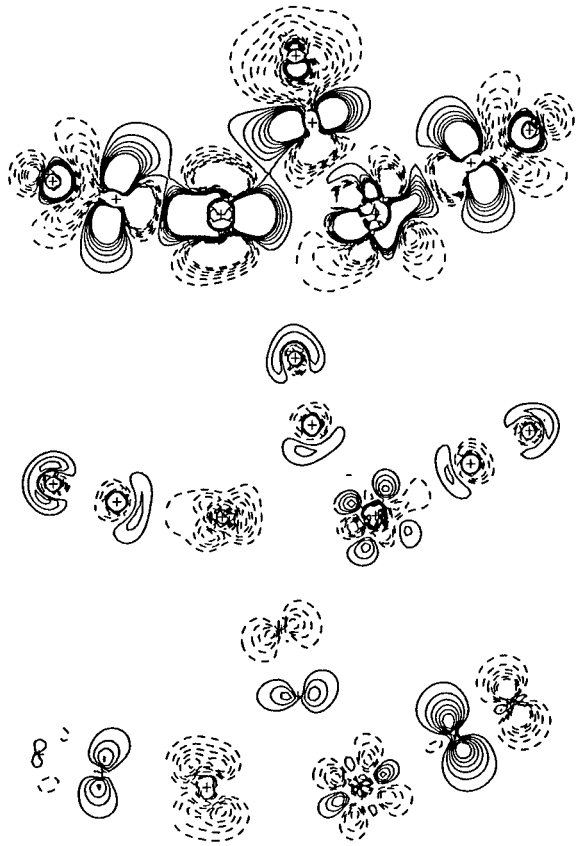

Figure 8. Density difference maps between the electron density computed at the Hartree−Fock, at the local spin density (DFT), and at the configuration interaction levels. (a, top) DFT − HF; (b, middle) DFT(gradient corrected) − DFT; (c, bottom) CI − HF. Zero contour not represented. Contour interval: 0.01e/Å^{-3}. No more than six positive and negative contours have been represented.

local spin density, LSD), and gradient-corrected DFT levels of calculation, using the same basis sets for all calculations.

As in Figure 7, the contours are plotted in the plane containing the two Rh atoms and the three carbonyls. Figure 8a presents the LSD − HF electron density difference contours. Note that the contour interval in Figure 8 is 0.001 e/Å^{-3}, compared to 0.1 e/Å^{-3} for Figure 7a and 0.05 e/Å^{-3} for Figure 7b. Since DFT and HF densities have been calculated using the same basis sets, this map is assumed to account for the change in the density distribution induced by electron correlation, the *correlation density*. Since the map of Figure 8a displays an increase of the π density at the carbon atoms and a concomitant decrease of the density at the π donating metal orbitals, it is tempting to conclude at a better balance of π back-donation interactions, a well-documented consequence of introducing electron correlation. However, a comparison with the work of Wang and colleagues[43] shows that the charge difference between LSD and HF displayed in the present work at the level of the carbonyl ligand is quite similar to that obtained on the isolated carbon monoxide molecule (see Figure 2a of ref 43, and note that the signification of dashed and solid lines is reversed with respect to that of Figure 8a in the present work). But, we now compare Figure 8a with the *deformation density map* of Figure 7a, keeping in mind that the contour interval of Figure 7a is 10 times larger. As discussed above, Figure 7 shows the deformation of the spherical atoms induced by bonding. It has been shown that most of this deformation should be attributed to the polarization of the density in the vicinity of individual atoms, or, in other words, to atomic hybridization.[47] A comparison between Figures 7 and 8a suggests that Hartree−Fock has gone too far in polarizing atomic density: density peaks tend to be smoothed away and depleted regions to be filled in. It could be concluded that the major effect in the reorganization of electron density induced by DFT with respect to HF is due to correlation at the atomic level, assuming that atoms are not anymore spherical, as in the standard promolecule, but "oriented" as proposed by Schwarz et al.[47] This atomic origin of the DFT − HF deformation is corroborated by Laidig,[44] who attributes the changes in the valence density distribution to a tightening of the atomic inner shells due to a decreased electron−electron repulsion.

It seems however that uncorrected DFT tends to overestimate those correlation effects. Figure 8b displays the density difference map between the BP method (gradient-corrected DFT) and the local spin density results. The solid lines denote an excess of BP electron density. The effect of gradient correction is much smaller than the LSD − HF difference, *and it is of opposite sign.* A similar trend has been obtained by Wang and colleagues on the CO molecule.[43]

Finally, Figure 8c displays the effect of *valence* correlation on the density distribution through a CI − HF difference map. The configuration interaction wave function has been obtained by correlating 38 electrons accommodated in outer valence metal orbitals with metal and metal/carbonyl character. Those 38 electrons have been correlated through a single reference singles-and-doubles CI expansion. The weight of the single reference in the CI expansion was 82%, and the retrieved correlation energy was 0.5338 hartree. This expansion is expected to correct the poor description of the π-back-donation characteristic of Hartree−Fock wave functions. Figure 8c confirms that most of the density reorganization is effectively restricted to the π orbitals of metal and carbonyls, with a population transfer from both metals—and, to some extent, from the oxygen atoms—to the π orbital of the carbon atoms. As far as π orbitals are concerned, this transfer is qualitatively similar to what was observed in the LSD − HF map, *but it is quantitatively much more limited,* suggesting that the correlation of inner atomic electrons, accounted for in LSD calculations, has a deeper influence on the reorganization of the density distribution.

Acknowledgment. Calculations have been carried out in part on a series of IBM RISC 6000 workstations purchased with funds provided by DGICYT (Project PB92-0766-C02-02) and by CIRIT of the Generalitat de Catalunya (Grant GR9Q93-7003), in part on a CRAY-YMP of the Centre de Supercomputació de Catalunya (Barcelona, Spain), and in part on the Cray-C98 computer of the IDRIS Center (CNRS, Orsay, France). The cooperation between the Strasbourg and Tarragona groups has been supported by the HCM network Contract ERBCHRXCT-930156. We are pleased to thank Professor R. F. W. Bader for a copy of the AIMPAC package of programs.

IC9505256

(47) (a) Kunze, K. L.; Hall, M. B. *J. Am. Chem. Soc.* **1986**, *108*, 5122; **1987**, *109*, 7617. (b) Schwarz, W. H. E.; Valtazanos, P.; Ruedenberg, K. *Theor. Chim. Acta* **1985**, *68*, 471. (c) Schwarz, W. H. E.; Mensching, L.; Valtazanos, P.; von Niessen, W. *Int. J. Quantum Chem.* **1986**, *29*, 909; **1986**, *30*, 439. (d) Schwarz, W. H. E.; Ruedenberg, K.; Mensching, L. *J. Am. Chem. Soc.* **1989**, *111*, 6926. (e) Mensching, L.; von Niessen, W.; Valtazanos, P.; Ruedenberg, K. Schwarz, W. H. E. *J. Am. Chem. Soc.* **1989,** *111,* 6933.